Supporting Information for "InP-$In_xGa_{1-x}As$ Core-Multi-Shell Nanowire Quantum Wells with Tunable Emission in the 1.3 – 1.55 µm Wavelength Range"

H. A. Fonseka,[1*] A. S. Ameruddin,[1, 2] P. Caroff,[1*] D. Tedeschi,[3] M. De Luca,[3] F. Mura,[4] Y. Guo,[1] M. Lysevych,[5] F. Wang,[1] H. H. Tan,[1] A. Polimeni[3] and C. Jagadish[1]

[1]*Department of Electronic Materials Engineering, Research School of Physics and Engineering, The Australian National University, Canberra, ACT 2601, Australia*

[2]*Faculty of Science, Technology and Human Development, Universiti Tun Hussein Onn Malaysia, Parit Raja, 86400, Batu Pahat, Johor, Malaysia*

[3] *Dipartimento di Fisica and CNISM, Sapienza Università di Roma, Piazzale A. Moro 2, 00185 Roma, Italy*

[4] *Dipartimento di Scienze di Base e Applicate per l'Ingegneria, Sapienza Università di Roma, Via Scarpa 16, 00185 Roma, Italy*

[5]*Australian National Fabrication Facility, Research School of Physics and Engineering, The Australian National University, Canberra, ACT 2601, Australia*

*Corresponding authors: a.fonseka.1@warwick.ac.uk, CaroffP@cardiff.ac.uk

Section 1: Experimental details pertaining to the growth of InP- $In_xGa_{1-x}As$ QWs

InP nanowire core: The InP nanowire cores were seeded by 50 nm colloidal Au particles. The Au particle-deposited InP (111)B substrates were heated to the growth temperature of 450˚C. Substrates were not annealed prior to growth, but TMIn was pre-flown for 15 s before initiating the growth. This pre-flow step reduces the non-vertical nanowire growths that arise from lack of alloying when the pre-growth annealing step is avoided. The TMIn and PH_3 flows were 1.62×10^{-5} and 5×10^{-3} mol/min, respectively. Nanowire core growth was carried out for 30 min at 100 mbar reactor pressure.

$In_xGa_{1-x}As$ QWs: After the core growth, the temperature was ramped up to the shell growth temperature of 550˚C and the reactor pressure was ramped to 180 mbar which was the pressure normally used in the current MOVPE system for InP-related planar vapour-solid epitaxial growth. The nanowire core was annealed for 3 min before depositing a thin InP buffer layer on the nanowire side facets in order to ensure a high quality surface for the subsequent QW growth. After a growth interruption of 5 s the QW growth was initiated. The TMIn, TMGa and AsH_3 flows used for the study of the effect of QW thickness variation were 6.75×10^{-6}, 5.51×10^{-6} and 1.34×10^{-3} mol/min, respectively, giving a vapour phase In molar fraction Xv = [TMIn]/([TMIn]+[TMGa]) of 0.55. The QW growth time was varied between 20 to 180 s depending on the targeted QW thickness. For the study of QW composition variation, the TMIn flow was kept constant at 6.75×10^{-6} mol/min while varying the TMGa flow to achieve compositions between GaAs and InAs, except in the case of GaAs, where the TMIn source was turned off. The growth time of these composition-varied QWs were also scaled accordingly in order to achieve a nominal thickness of 7 nm. Another 5 s growth interruption was included after the QW growth with AsH_3 left on in order to prevent As desorption from the thin QW [1]. Lastly, an InP barrier shell was grown for 12 min. For the growth of MQW structure, the QW, interruption and barrier growth steps were repeated two times more.

Fig. S1: TEM image of the nanowire QW showing stacking fault distribution along the nanowire

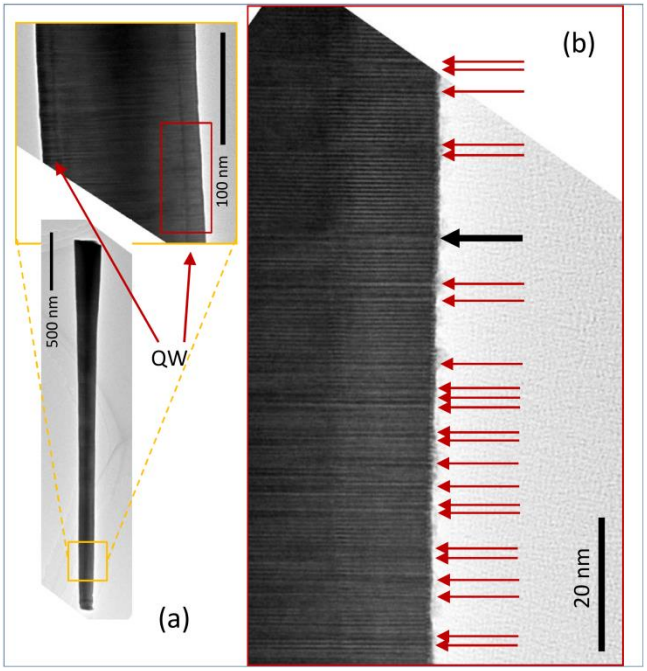

Fig. S1: (a) Low magnification TEM images showing the QW and the area used for the high magnification image. (b) High magnification TEM image showing the rather even distribution of stacking faults (indicated by red arrows). The black thick arrow indicates a ZB insert. All images are taken along <11-20> zone axis.

Table S1: Material parameters used to create WZ InP and InGaAs material for the QW emission wavelength simulation

Parameter	**InP**	**GaAs**	**InAs**	**Unit**
Lattice constant along a at 300 K	4.1423 [2]	3.9976 [3]	4.274 [4]	Å
Lattice constant along c at 300 K	6.8013 [2]	6.5281 [3]	7.025 [4]	Å
Direct energy gap at 300 K	1.421 [5]	1.437 [6] [1]	0.412 [7] [2]	eV
Electron effective mass along a	0.088 [8]	0.082 [8]	0.042 [8]	m_0
Electron effective mass along c	0.105 [8]	0.090 [8]	0.060 [8]	m_0
Hole effective mass along a	0.158 [8]	0.134 [8]	0.084 [8]	m_0
Hole effective mass along c	1.273 [8]	1.026 [8]	1.7 [8]	m_0
Elastic constants (C11,C12,C13,C33,C44)	120.3, 52.3, 40.7,131.9, 27.1 [9]	147.6, 46, 33.4, 160.2, 42.4 [10] [3]	100.3, 42.2, 31.8, 110.7, 23.0 [9]	GPa
Conduction band absolute deformation potential (a axis, c axis)	-3.14, -7.75 [11]	-3.75, -6.79 [12]	-3.83, -6.39 [11]	eV
Valence band uniaxial deformation potential (D1, D2, D3, D4, D5, D6)	-3.7, 4.5, 5.92, -3.28, -2.94, -5.5 [11]	-3.7, 4.5, 7.68, -3.84, -3.86, -5.5 [12]	-3.7, 4.5, 5.85, -3.17, -2.78, -5.5 [11]	eV

[1] Value at 290 K
[2] Assuming ZB Varshini parameters
[3] Assuming GaN values

Unstrained valence band alignment	1.15 [13, 14] [4]	1.56 [13, 15] [4]	1.565 [13, 16] [4]	eV

Table S1: WZ InP, GaAs and InAs material parameters used for QW emission wavelength simulation.

Section 2: Assumptions made in the theoretical simulation of emission wavelengths of WZ InP-InGaAs QWs

There are a number of aspects that have not been or cannot be considered in the theoretical simulations. Bowing parameters of WZ phase InGaAs are unknown. Hence, linear interpolation between available values of WZ GaAs and InAs are used except for conduction and valence bands. Some of the values used, for example the effective electron masses, are theoretical or based on ZB values, which could be different experimentally and/or in the WZ phase. Moreover, even the experimentally determined values such as band-gaps of WZ GaAs and InAs are also still under debate. There are also aspects such as strain relaxation which could be taking place, especially in the thicker QWs. Yet, it is considered to be uni-axial, coherent and fully strained in the calculations. Another structural observation that is not included in the simulations is the presence of stacking faults and the occasional thin ZB inclusions. These may lead to complex carrier separation in the axial and radial directions, spatially indirect transitions,[14] different peak energies and charge accumulation due to saw-tooth-like potential build-up due to spontaneous polarisation in WZ regions [15, 17-19] along the nanowire (WZ c-axis). The nanowire QW could also behave differently to the simulated planar QW due to its geometrical tube-like shape. For example it has been shown that ground state carriers can be confined to the apices of the facets [20, 21].

References:

1. M. Tabuchi, R. Takahashi, M. Araki, K. Hirayama, N. Futakuchi, Y. Shimogaki, Y. Nakano and Y. Takeda, *Applied Surface Science*, 2000, **159–160**, 250-255.

[4] By adding the relative WZ valence band offset of the same material to the absolute ZB valence band position

2. D. Kriegner, E. Wintersberger, K. Kawaguchi, J. Wallentin, M. T. Borgström and J. Stangl, *Nanotechnology*, 2011, **22**, 425704.
3. M. de la Mata, C. Magén, P. Caroff and J. Arbiol, *Nano Letters*, 2014, **14**, 6614-6620.
4. D. Kriegner, C. Panse, B. Mandl, K. A. Dick, M. Keplinger, J. M. Persson, P. Caroff, D. Ercolani, L. Sorba, F. Bechstedt, J. Stangl and G. n. Bauer, *Nano Letters*, 2011, **11**, 1483-1489.
5. A. Zilli, M. De Luca, D. Tedeschi, H. A. Fonseka, A. Miriametro, H. H. Tan, C. Jagadish, M. Capizzi and A. Polimeni, *ACS nano*, 2015, **9**, 4277-4287.
6. M. De Luca, G. Lavenuta, A. Polimeni, S. Rubini, V. Grillo, F. Mura, A. Miriametro, M. Capizzi and F. Martelli, *Physical Review B*, 2013, **87**, 235304.
7. M. B. Rota, A. S. Ameruddin, H. A. Fonseka, Q. Gao, F. Mura, A. Polimeni, A. Miriametro, H. H. Tan, C. Jagadish and M. Capizzi, *Nano Letters*, 2016, **16**, 5197-5203.
8. A. De and C. E. Pryor, *Physical Review B*, 2010, **81**, 155210.
9. M. W. Larsson, J. B. Wagner, M. Wallin, P. Håkansson, L. E. Fröberg, L. Samuelson and L. R. Wallenberg, *Nanotechnology*, 2006, **18**, 015504.
10. I. Vurgaftman and J. R. Meyer, *Journal of Applied Physics*, 2003, **94**, 3675-3696.
11. c. Hajlaoui, L. Pedesseau, F. Raouafi, F. B. CheikhLarbi, J. Even and J.-M. Jancu, *Journal of Physics D: Applied Physics*, 2013, **46**, 505106.
12. T. Cheiwchanchamnangij and W. R. L. Lambrecht, *Physical Review B*, 2011, **84**, 035203.
13. S.-H. Wei and A. Zunger, *Applied Physics Letters*, 1998, **72**, 2011-2013.
14. K. Pemasiri, M. Montazeri, R. Gass, L. M. Smith, H. E. Jackson, J. Yarrison-Rice, S. Paiman, Q. Gao, H. H. Tan, C. Jagadish, X. Zhang and J. Zou, *Nano Letters*, 2009, **9**, 648-654.
15. N. Vainorius, D. Jacobsson, S. Lehmann, A. Gustafsson, K. A. Dick, L. Samuelson and M.-E. Pistol, *Physical Review B*, 2014, **89**, 165423.
16. J. K. Panda, A. Chakraborty, D. Ercolani, M. Gemmi, L. Sorba and A. Roy, *Nanotechnology*, 2016, **27**, 415201.
17. L. Li, Z. Gan, M. R. McCartney, H. Liang, H. Yu, W.-J. Yin, Y. Yan, Y. Gao, J. Wang and D. J. Smith, *Advanced Materials*, 2014, **26**, 1052-1057.
18. U. Jahn, J. Lähnemann, C. Pfüller, O. Brandt, S. Breuer, B. Jenichen, M. Ramsteiner, L. Geelhaar and H. Riechert, *Physical Review B*, 2012, **85**, 045323.
19. B. Bauer, J. Hubmann, M. Lohr, E. Reiger, D. Bougeard and J. Zweck, *Applied Physics Letters*, 2014, **104**, 211902.
20. M. Fickenscher, T. Shi, H. E. Jackson, L. M. Smith, J. M. Yarrison-Rice, C. Zheng, P. Miller, J. Etheridge, B. M. Wong, Q. Gao, S. Deshpande, H. H. Tan and C. Jagadish, *Nano Letters*, 2013, **13**, 1016-1022.

21. M. Heigoldt, J. Arbiol, D. Spirkoska, J. M. Rebled, S. Conesa-Boj, G. Abstreiter, F. Peiro, J. R. Morante and A. Fontcuberta i Morral, *Journal of Materials Chemistry*, 2009, **19**, 840-848.